# Molecular beam epitaxy of compound materials through shadow masks

T. Schallenberg and L. W. Molenkamp
*Physikalisches Institut, Experimentelle Physik III, Universität Würzburg, D-97074 Würzburg, Germany*

G. Karczewski
*Institute of Physics, Polish Academy of Sciences, Al. Lotników 32/46, 02-668 Warszawa, Poland*
(Received 6 April 2004; published 29 October 2004)

We present a consistent model for growth dynamics in molecular beam epitaxy of compound materials through shadow masks. The model takes into account specific properties of II-VI and III-V material systems. In the case of the II-VI compounds, the redistribution of molecular fluxes under the shadow masks plays a crucial role. Based on the model, we show that reactions between the constituent species determine the flux distribution within the mask cavity, which also affects the deposition of compound material. In contrast, for III-V materials surface diffusion is the key factor responsible for the shape of the deposits. Our model considers also that the diffusing species interacts with the molecular flux of the other constituent. Hence, surface diffusion of group-III atoms is controlled by the influx of group-V species, which in turn is determined by the growth geometry. In addition, we demonstrate that surface diffusion takes place in absence of group-III flux. The formation of the deposits in characteristic shapes, observed in our experiments, can also be explained based on the model.

DOI: 10.1103/PhysRevB.70.155328 PACS number(s): 68.43.−h, 81.15.Aa, 81.07.−b, 81.15.Hi

## I. INTRODUCTION

Molecular beam epitaxy (MBE) using shadow masks is a versatile selected area epitaxy (SAE) technique for the fabrication of modulated semiconductor heterostructures. Several studies have demonstrated the potential of this method to fabricate novel devices. Examples are (1) the lateral integration of optical elements and quantum structures,[1–4] which can be used to fabricate, e.g., integrated full-color emitters; and (2) selective contacts to embedded structures, such as doping superlattices[5] and electron gases.[6]

Recently, we demonstrated that shadow mask assisted growth is particularly interesting for the fabrication of compound semiconductor nanostructures.[7] Employing epitaxial shadow masks, quantum structures such as single quantum dots and quantum wires can be reproducibly grown with a spatial accuracy of the order of 10 nm. The key controlling factors in SAE growth of compound semiconductors using shadow masks are (1) the incidence angles of the molecular beams and (2) the shape of the shadow mask itself. The versatility of this method is enhanced by choosing appropriate variants of the technique for specific applications as was reported recently.[8]

The application of this interesting method, however, requires an understanding of the fundamentals of the growth process. There are a few reports on the various aspects of the growth mechanism in shadow mask assisted MBE of compound semiconductors.

Tomita *et al.* investigated the shadow mask assisted MBE of GaAs.[9] Self-formation of low-index facets takes place at the edge of the grown GaAs structures, which is limited by the incidence of Ga on the substrate. Diffusion of Ga adatoms out of the incidence region is caused by the lateral gradient of the surface concentration of adsorbed Ga adatoms and the self-formation of low-index facets can be explained (and modeled) by the fact that the surface lifetime of adatoms depends on the surface orientation.

Nishikawa *et al.* investigated shadow masked MBE of ZnSe with compound source material and observed that ZnSe grows also on the backside of the mask.[10] This was attributed to surface diffusion and a diffusion length of 0.5 $\mu$m was extracted from the experiments. In another study, MBE growth of ZnSe with nonparallel incidence of Zn and Se beams has been investigated.[11] The formation of a shoulder structure in the incidence region of Se has been observed. This was explained by the diffusion of Zn into the region where only Se (no Zn) impinges on the substrate.

In the present contribution, it is proposed that contrary to the previous suggestions, shadow mask assisted growth of ZnSe can be understood to occur without invoking surface diffusion of adatoms. The experimental observations can be explained by the unique growth regime within the cavity of the mask, where molecules can be desorbed and adsorbed many times without leaving the cavity. By modeling this repetitive redistribution process, one calculates the effective flux distribution in the steady state. The results accurately describe the effects observed in the experiments with ZnSe growth.

In this work, the effects of surface diffusion in shadow mask assisted growth of compound materials are also modeled. In principle, the diffusion model used by Tomita *et al.* is not specific to compound materials, because it does not consider the effects of the group-V flux.[9] However, Hata *et al.* has demonstrated that the surface diffusion length of group-III adatoms strongly depends on the anion flux.[12] This effect is included in the model and the important consequences on the SAE of III-V compounds are discussed.

Below, we first present results of MBE growth of ZnSe, InAs, and GaAs compounds using shadow masks. Next, we describe the model, starting from the growth of single-component and two-component materials, where we assume that the fluxes of the constituents are independent; i.e., the species do not react with each other. Subsequently, we ex-

 

pand the model to compound materials where the interaction between the constituent species plays a crucial role. Because the constituents react with each other on the surface, their flux distributions depend on each other. In addition to the interaction between the fluxes of the constituents, we include the interaction between the redistribution of the fluxes via multiple desorption on the one hand and surface diffusion on the other hand in the model. In the final discussion, we model the shapes of the deposits from growth experiments with II-VI and III-V materials and explain the observations. In addition, we discuss some important implications of the interaction between the constituent species of a compound material on the SAE using shadow masks.

## II. EXPERIMENTS

In order to test the predictions of the model, we compare them with the observations of our experiments, wherein ZnSe (GaAs) was grown through a shadow mask using different growth parameters. In these experiments, the shadow masks were fabricated from GaAs/AlGaAs epitaxial layers grown on a GaAs (001) substrate, consisting of a $h=1.27\ \mu$m (1.16 $\mu$m) thick $Al_{0.6}Ga_{0.4}As$ spacer and a $g=400$ nm (140 nm) thick GaAs cap. Conventional photolithography and wet chemical etching were employed to open stripe apertures (10 mm long and $w=1-10\ \mu$m wide) oriented along [110] and $[1\bar{1}0]$ direction in the GaAs cap layer. Subsequently, the AlGaAs spacer below the apertures was removed by selective etching in hydrofluoric acid. Etching was allowed to proceed until the cap layer was undercut over a distance of $u=2-4\ \mu$m. Thus, a shallow mask cavity with freestanding shadow edges was obtained (see Fig. 4). In order to investigate the role of the crystal orientation on shadow mask assisted growth, two patterned samples with different crystal orientation [aperture stripe parallel (110) and $(1\bar{1}0)$] were overgrown in the second epitaxial growth.

### A. II-VI compounds

Experiments on II-VI MBE were done in a RIBER 32 growth chamber, which is equipped with solid source effusion cells. High purity (6N) materials (Zn; Cd; Se) were used for the growth. The growth conditions were slightly modified in order to reduce the width of the partial shadow of the beam (due to the finite size of the source): The apertures of the effusion cells were capped with pyrolytic boron nitride disks, leaving only 2-mm holes in the middle. We observed that the introduction of these beam plates reduced the width of partial shadows to ~20 nm. MBE growth of the ZnSe layers was carried out at a substrate temperature of 280 °C and a beam equivalent pressure (BEP) of $5\times10^{-7}$ Torr for Zn, while the Se flux was varied. For experiments #1 to #4 the flux ratios $BEP_{Zn}/BEP_{Se}$ were set to 0.28, 0.75, 2.5, and 0.19, respectively. Sample #4 was grown in a later experiment without the beam plates. Therefore, partial shadow effects are observed in this case. The dimensions of the shadow mask are $h=2.77\ \mu$m, $g=280$ nm, and $u=1\mu$m, while the width $w$ of the apertures was varied from 1 to 6 $\mu$m for different stripes. By this means, we can verify the predictions of the model regarding the mask geometry.

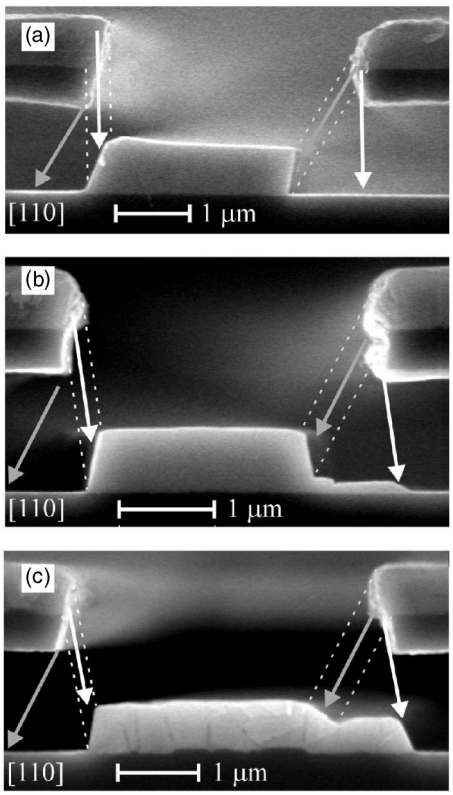


FIG. 1. Electron micrographs of the cleaved edge of an epitaxial shadow mask (dark material), which was overgrown with ZnSe (bright material). The incidence directions of Se (white) and Zn (gray) are indicated by the arrows. The three micrographs (a), (b), and (c) represent ZnSe growth with increasing Zn:Se flux ratio.

Figure 1 shows cross-sectional scanning electron micrographs (SEM) of the cleaved edge of samples #1, #2, and #3. Due to the material contrast, the darker GaAs substrate and the overhanging GaAs cap can be distinguished from the bright ZnSe structures, which were grown in the experiments. This contrast would also identify structures from elemental Zn or Se (which are not expected because of the high vapor pressure of the elements at growth temperature). ZnSe was grown both onto the mask and through its apertures. ZnSe was also deposited on the sides of the aperture and the backside of the mask (as in Ref. 10), albeit with lower growth rates.

As can be seen in Fig. 1(a) [sample #1], the ZnSe structure on the substrate was selectively grown in the overlap of the incidence regions of the component beams (*overlap region*). The beam directions are indicated by the gray (Zn) and white (Se) arrows. Because of the different angles of incidence (+26° and −2°), the width of the growth area is smaller than the aperture of the mask. When the Se:Zn flux ratio is decreased [see Fig. 1(b), sample #2], ZnSe grows at a lower growth rate also in the region where only Se beam impinges on the substrate (*Se domain*). The growth rate of this shoulder structure increases when the Se:Zn flux ratio is further decreased [see Fig. 1(c), sample #3] and its thickness becomes similar to the main structure in the overlap region.

On the other hand, with a high Se overpressure (sample #4) ZnSe grows in the entire incidence region of Zn; i.e., a shoulder is formed in the *Zn domain*.

In addition, ZnSe growth rates depend also on the geometry of the mask. For example, in the case of sample #4, the thickness of the shoulder structure $R_{Zn}$ decreases when the aperture width is increased [see Fig. 7, sample #4]. Parallel to this, the growth rate $R_0$, outside the incidence regions of Zn and Se beams, i.e., without a direct flux, is increased.

These results can hardly be explained by surface diffusion. Another indication that diffusion effects do not shape the profile of the ZnSe structures is the shape of the edges. For fully open Knudsen cells, round edges are formed because of the flux gradient of the partial shadow.[13] However, in the case of samples #1, #2, #3, the width of the partial shadow region has been reduced to ~20 nm by employing the beam plates. As can be seen in Fig. 1, the edges of the ZnSe structures are quite smooth with steep inclination angles, which evidently do not correspond to a low-index crystal plane. The inclination of the facets can be explained, geometrically, by the deposition of material on the cap layer of the shadow mask, leading to a gradual closure of the apertures. This is illustrated by the dashed lines in Fig. 1, which indicate the limits of the overlap region at the beginning and the end of ZnSe growth. As can be seen, the inclination of the edges of the ZnSe structures is determined by the closing of the aperture. Under certain conditions, even overhangs are created [see Fig. 1(a)]. In addition to these higher index facets, we have also observed the self-formation of low-index (111) facets. This occurs selectively when ZnSe is grown through a mask with the aperture stripe oriented parallel to $(1\bar{1}0)$ direction and when the Se:Zn flux ratio is high (samples #1, #4). Otherwise, no low-index facets are formed (samples #2, #3). ZnSe structures with (111) facets are still restricted to the geometrically defined growth area. Thus, the self-formation of low-index facets implies that the volume of the ZnSe structure is reduced. Therefore this process is not driven by surface diffusion, but by the reduced deposition rate (sticking coefficient) on a (111)A facet. This is different from shadow-masked growth of GaAs, where low-index facets are formed by intersurface diffusion.[9]

In summary, the investigation of shadow-masked growth of ZnSe has not shown indications of surface diffusion of adatoms shaping the profile of SAE grown structures on the scale of ~20 nm. The origin of experimental observations such as the dependence of the growth rates on the fluxes and the geometry of the mask, can be explained by the model below, which considers an unique growth regime in the mask-cavity.

### B. III-V compounds

When III-V materials are grown using a shadow mask, the growth kinetics are quite different from those of the II-VI materials. Surface diffusion is the key factor that governs the shape of III-V deposits, because the diffusion lengths of group-III adatoms on the surface of a growing III-V layer may exceed 1 $\mu$m.[12] Because of the low vapor pressure of the group-III elements, their sticking coefficient $s_{III}$ is close to unity at normal growth conditions and is almost independent of the group-V flux. This is in contrast with II-VI MBE, where the sticking coefficients of the constituents depend on the flux of the other constituent species.[14]

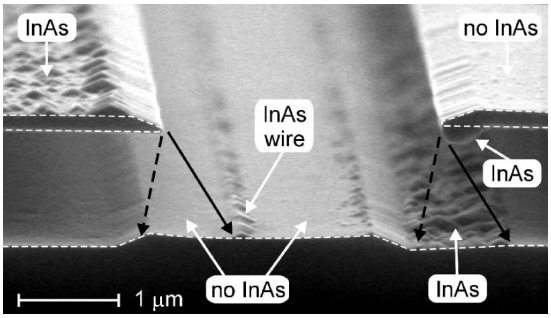


FIG. 2. Electron micrograph of an epitaxial shadow mask with InAs deposits. White dashed lines indicate the interface of the GaAs substrate and the mask. The black arrows indicate the incidence directions of In (dashed line) and As (solid line).

Figure 2 demonstrates that the specific properties of the III-V materials, discussed above, result in a very different growth process when they are deposited through a shadow mask. The SEM image shows a shadow mask sample with GaAs and InAs deposits. The III-V structures were grown in a RIBER 32 growth chamber, equipped with solid source effusion cells and high purity (6N) source materials (Ga; In; As). The arsenic source is a valved cracking cell where the thermal cracking zone is maintained at 560 °C. Therefore, the arsenic flux consists of $As_4$ molecules mainly. In the experiment, the widths of the partial shadows of the As, Ga, and In beams are about 100, 200, and 200 nm, respectively. First, a 150 nm thick GaAs buffer was grown at substrate temperature of 580 °C with Ga and As BEPs of $5.0\times10^{-7}$ and $3.4\times10^{-6}$ Torr, respectively. The configuration was such that both beams impinged at an angle of incidence of $\varphi=+9°$. The white dashed lines in Fig. 2 indicate the interface of the epitaxial shadow mask with the GaAs buffer, before the deposition of InAs. Subsequently, a nominally 18 nm thick InAs layer was grown at a substrate temperature of 480 °C with In and As BEPs of $6.3\times10^{-7}$ and $8.0\times10^{-6}$ Torr, respectively. This was carried out in a such configuration that In impinged at $\varphi_{In}=+11°$ (see black dashed arrows) directly onto the area of the GaAs buffer, while As impinged at $\varphi_{As}=-33°$ (see black solid arrows), hence the incidence region is offset to the right by a distance of ~1.0 $\mu$m. Because InAs grows in the Stranski-Krastanov growth mode, the deposits form three-dimensional (pyramidal) structures, which can be easily identified in Fig. 2. In addition, the InAs structures are distinguishable from the GaAs structures by the material contrast in SEM images.

As can be seen in Fig. 2, InAs pyramids have grown in the As domain, i.e., on the right-hand side of the GaAs buffer, although no In atoms impinged in this region. On the other hand, in most of the incidence region of the In beam no three-dimensional deposits can be observed. The only significant InAs growth rate in the incidence region of indium adatoms coincides with the left limit of the incidence region of the arsenic beam, where a InAs wire structure has been formed. These observations demonstrate that the shadow

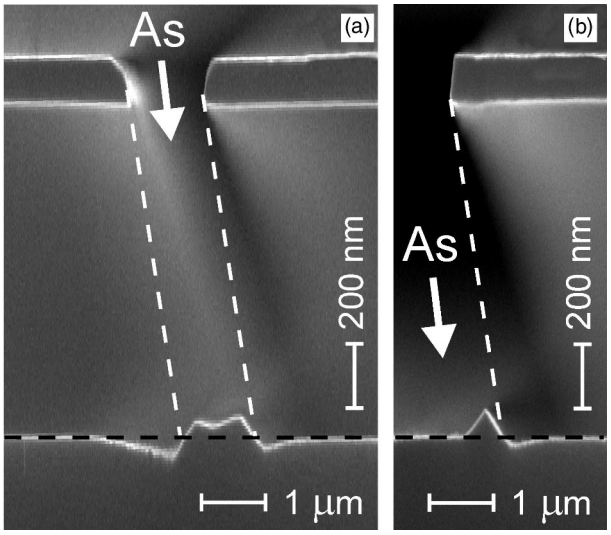


FIG. 3. Electron micrographs of the cleaved edge of an epitaxial shadow mask, with different aperture widths of (a) 1.2 $\mu$m and (b) 7.0 $\mu$m. Surface diffusion, which causes the modulation of the substrate surface, was activated thermally. The lateral modulation coincides with the incidence of As through the aperture of the mask, as indicated by the white lines. The black line indicates the interface of the GaAs substrate before the thermal process.

mask assisted growth of II-VI and III-V compounds are governed by very different processes. In addition, the deposition on top of the mask is different for II-VI and III-V compounds. As shown in Fig. 2, InAs deposits are clearly visible on the left wing of the mask, whereas only a negligible amount of InAs is observed to have deposited onto the right wing. In contrast, some deposition can be seen on the backside of the right wing of the mask. These features can be explained by surface diffusion phenomena, resulting from the interactions between the constituent species of compound materials. Such effects may also be important for the growth of III-V materials on patterned substrates.

In order to investigate the effects of the group-V flux on the surface diffusion of group-III adatoms, we fabricated a sample by a thermal process that does not employ group-III fluxes. Similar to the previous experiments, a shadow mask sample consisting of a GaAs/AlGaAs epitaxial shadow mask on a GaAs (001) substrate was loaded in the growth chamber and the native oxide layer was desorbed at 580 °C. Subsequently, the sample was tempered at 630 °C for 10 min, and, finally cooled to 300 °C. During the entire process, the arsenic beam (BEP: $1.2\times10^{-5}$ Torr) was so adjusted that it impinged on the GaAs substrate through the apertures of the mask at an angle of −11°.

Figure 3 shows cross-sectional SEM images of the cleaved $[\bar{1}10]$ edge of the GaAs sample. The image is magnified in the growth direction in order to exhibit the details of the shallow structures, which were formed during the thermal treatment. The white lines in Fig. 3 indicate the incidence direction of the arsenic beam, while the black lines indicate the original surface of the GaAs substrate, before the thermal treatment. Obviously, tempering of the sample with arsenic flux modifies the GaAs interface. In the incidence region of the arsenic beam, GaAs is accumulated, while grooves were formed on either side [see Fig. 3(a)]. Almost the same effects are observed for the growth assisted by shadow masks with the [110] orientation of the stripe aperture. However, the edges of the GaAs deposits exhibit (111)B and (001) faceting instead of (114)A, which is observed in Fig. 3.

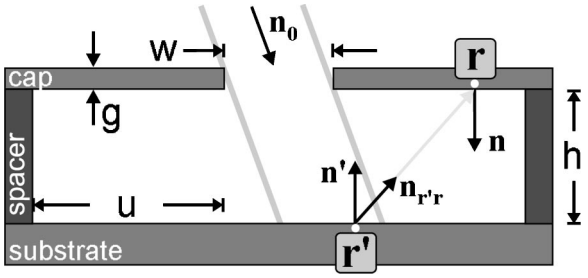


FIG. 4. Sketch of an epitaxial shadow mask. Gray lines indicate the limits of a direct molecular beam passing through the mask aperture. The dimensions and vectors were used in modeling the growth regime within the cavity of the mask.

Since no external Ga fluxes were employed in the experiment, it can be unambiguously concluded that Ga atoms migrate from the outside to the inside of the incidence region of the arsenic beam on the substrate. The effect is restricted to the region near the step-edge of the arsenic flux, as is clearly seen in Fig. 3(b), where the width of the aperture was 7 $\mu$m. Obviously, the incidence of the arsenic flux governs the surface diffusion of the Ga atoms, as is discussed below.

## III. MODEL

### A. Single-component material

Before analyzing the SAE growth of compound semiconductors, we restrict ourselves to a simplified case wherein we consider only the flux ($p_0$) of a single species. After passing through an aperture of the mask, the impinging particles are adsorbed on a restricted area on the substrate, which is the projection of the aperture cross section (between the gray lines in Fig. 4). The lateral position of this incidence region is determined by the incidence direction $\mathbf{n}_0$ of the beam. Adsorbed species have a finite lifetime $\tau$ on the substrate surface after which the material either is incorporated into the growing crystal or desorbs and goes elsewhere. The probability of incorporation of the constituent elements is given by the sticking coefficient $s$, which is a constant parameter, when there are no local variations of temperature and no interaction between different species.

Nonsticking molecules $(1-s)$ are subsequently reemitted from the surface with an angular distribution given by the cosine law of effusion. This redistribution process contributes to higher order fluxes $F_k$ (of the order $k>1$) because the re-desorbed molecules, which do not leave the cavity through an aperture, impinge on other surface of the cavity. This process is iterative: The redistribution of these nonsticking, $k$th-order molecules $(1-s)F_k$ gives an $(k+1)$th-order flux $F_{k+1}$, where we define $F_0$ as the direct flux, i.e., the primary flux from the source. $F_0$ is equivalent to $p_0$ for po-

sitions $\mathbf{r}$ within the incidence region and it is zero outside. Thus, the total flux $f$ is given by

$$f(\mathbf{r},t) = \sum_{k=0}^{\infty} F_k(\mathbf{r},t), \tag{1}$$

where the time dependence $t$ corresponds to the finite surface lifetime $\tau$ of adsorbed molecules; i.e., the iteration of the redistribution process is equivalent with time. Accordingly, the redistribution of nonsticking molecules after each collision is given by the equation[15]

$$F_{k+1}(\mathbf{r},t+\tau) = \int_{A_M} [1 - s(\mathbf{r}',t)] F_k(\mathbf{r}',t) Z(\mathbf{r},\mathbf{r}') \times \frac{(\mathbf{n}_{\mathbf{r}'\mathbf{r}} \cdot \mathbf{n}')(\mathbf{n}_{\mathbf{r}\mathbf{r}'} \cdot \mathbf{n})}{(\mathbf{r}-\mathbf{r}')^2 \pi} dA', \tag{2}$$

where $\mathbf{n}'$ ($\mathbf{n}$) is the unit normal to the surface element at $\mathbf{r}'$ ($\mathbf{r}$) and $\mathbf{n}_{\mathbf{r}'\mathbf{r}}(=-\mathbf{n}_{\mathbf{r}\mathbf{r}'})$ is a unit vector pointing to $\mathbf{r}$ from $\mathbf{r}'$ (the scalar products of the unit vectors are the cosines of the effusion and incidence angles). $A_M$ is the surface area of the mask cavity and $Z(\mathbf{r},\mathbf{r}')$ is equal to 1 as long as there is line of sight between the surface elements at $\mathbf{r}'$ to $\mathbf{r}$, and $Z$ is zero, if $(\mathbf{n}_{r'r} \cdot \mathbf{n}')$ is negative.

When the primary flux from the source $F_0(\mathbf{r})$ is time independent, the total flux $f(\mathbf{r},t)$ approaches a steady state distribution $f_\infty(\mathbf{r})$. In the case of noninteracting species, where the sticking coefficient $s$ is constant, $f_\infty$ is easily calculated using Eqs. (1) and (2).

Figure 5(a) shows a typical result. $f_\infty$ has been calculated for an ideal mask with typical dimensions $w=2$ $\mu$m, $h=2$ $\mu$m, and $u=4\mu$m (and idealized $g=0$ $\mu$m) and considering a single direct beam (flux $p_0$) impinging through the aperture of the mask at an angle of $\varphi=-14.0°$ (see Fig. 4). The incidence region of the beam is therefore shifted (by $\Delta x=+0.5$ $\mu$m) relative to the aperture of the mask [*Because of only angular dependence of the redistribution process, no absolute dimensions are required (scalability of the mask) and the units* ("$\mu m$") *will therefore be omitted below*.]

The three curves in Fig. 5(a) show the steady state flux distributions $f_\infty(\mathbf{r})$ for molecules with sticking coefficients $s=0.02$, 0.1, and 0.5, respectively ($f_\infty$ is normalized with respect to the primary flux $p_0$). The horizontal axis is the lateral position $x$ on the substrate surface. One clearly observes that $f_\infty$ is nonzero outside the incidence region of the direct beam. This is due to the repetitive adsorption and reemission process, where higher order impingements ($k \geqslant 1$) contribute to the *secondary flux* $F_\infty=(f_\infty - F_0)$, within the mask cavity. This contribution is large for a small sticking coefficient; i.e., when the probability of the molecules being desorbed multiple times is high. However, $F_\infty$ is limited by (1) the impingement rate of molecules, i.e., the beam pressure $p_0$; and (2) the escape rate of molecules through the aperture of the mask. The latter causes a disruption of the secondary flux near the aperture [see dashed curve in Fig. 5(a)]. On the other hand, $F_\infty \approx p_0$ ($f_\infty \approx 2p_0$) when the sticking coefficient is negligibly small ($s \approx 0$) and only few molecules escape through the aperture; i.e., for a mask with small $w$ and large $h$ or near the end walls of the mask cavity.

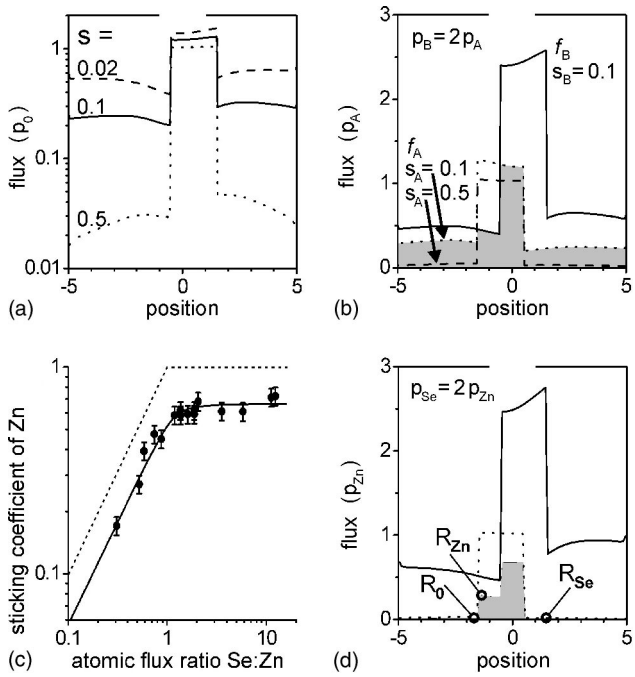


FIG. 5. Modeling of the total flux as a function of the lateral position below a shadow mask. (a) Total flux of a single molecule beam ($p=1$) with constant sticking coefficients $s=0.5$, 0.1, and 0.02. (b) Total flux of two molecule beams (dotted line: $p_A=1$; $s_A=0.1$; solid line: $p_B=2$, $s_B=0.1$) without considering the interaction of the fluxes. The gray shaded area is an estimate of the growth rates when growth is limited by the smaller flux. The dashed line represents a higher sticking coefficient $s_A=0.5$. (c) Material properties of ZnSe MBE growth (at 300 °C) from the literature: Sticking coefficient of Zn dependent on the Se:Zn flux ratio. (d) Total flux of interacting Zn flux (dotted line: $p_{Zn}=1$) and Se flux (solid line: $p_{Se}=2$). The gray shaded area is the modeled ZnSe growth rate as a function of the lateral position below the shadow mask. From the growth profile, the normalized growth rates $R_{Se}$ (Se shoulder), $R_{Zn}$ (Zn shoulder), and $R_0$ (without direct beam) were extracted for the data presented in Fig. 7.

### B. Two-component material

Next, we calculate the steady state flux distribution of two fluxes ($p_A$ and $p_B=2\times p_A$) with the beams impinging at different angles ($\varphi_A=+14.0°$ and $\varphi_B=-14.0°$). Below, we name the two species *minority* and *majority*, which refers to the different impingement rates $p_A$ and $p_B$, respectively. Again, we assume that the molecules do not interact. The dotted and solid lines in Fig. 5(b) show the total fluxes $f_A$ and $f_B$ (normalized to $p_A$) for constant sticking coefficients $s_A=s_B=0.1$. In this case, the flux of the majority species is dominant ($f_B > f_A$) within the cavity of the mask, except in the incidence region of the minority species ($f_B < f_A$); i.e., in the part where the direct beam of the majority species does not impinge. This local inversion of the flux ratio is important when compound semiconductors are grown because the growth rate is limited by the smaller of the two component fluxes.

This constraint can be used as a first order approximation of the growth rate, as is illustrated by the shaded area in Fig. 5(b). In steady state, the growth rate is at maximum in the overlap region. Outside this area, the growth rate is nonzero because of the coexistence of secondary fluxes of both species. The deposition rate is limited by the (small) secondary flux of the minority species; except in the domain of the minority species, where the flux ratio $f_B:f_A$ is the reverse. A shoulder structure is formed, because the growth rate is limited by the (large) secondary flux of the majority species.

This serves as a qualitative explanation for the observation that a shoulder structure is selectively formed in the domain of the minority species when ZnSe is grown with a high flux ratio [samples #3, #4]. In the case of sample #1, no shoulder structure formed because of stoichiometric growth conditions ($p_A \approx p_B$), i.e., $F_{Se} \approx F_{Zn}$; still, the reflection high-energy electron diffraction (RHEED) pattern revealed a "Se-rich" $(2\times1)$ reconstruction during the ZnSe growth. The latter can be explained by the fact that the phase transition between $(2\times1)$ and $c(2\times2)$ reconstruction takes place at an *atomic flux ratio* $p_{Se}:p_{Zn} \approx 0.7$.[16] In the case of sample #2, both reconstruction patterns were observed during ZnSe growth, reflecting a Zn-rich growth condition. Therefore, a shoulder structure was formed in the Se domain [see Fig. 1(b)].

This demonstrates that the local reversal of the flux ratio is the origin of the formation of a shoulder structure in the domain of flux of the minority species. However, the assumption of a constant sticking coefficient does not yield a quantitative prediction of the growth rates. In particular, the estimated growth rate without a direct beam [for $s=0.1$; see Fig. 5(b)] is an order of magnitude larger than that observed in the experiments. A better agreement with the experiment is obtained only if the sticking coefficient of the minority species is assumed to be larger than that of the majority species [e.g., $s_A=0.5$; see dashed line in Fig. 5(b)]. This behavior cannot be attributed to a difference in the material properties of the two species, but rather can be understood by considering the interaction of the fluxes, as explained in the next section.

### C. Two interacting fluxes

An interaction between the fluxes $f$ implies that the sticking coefficient $s$ would depend on the fluxes $f$ of both species. For a binary semiconductor AB the atomic incorporation rate $S$ is given by $S=sf$, and it is equal for both A and B since the stoichiometry of the compound is restored. As a result of this, the sticking coefficients $s_A$ and $s_B$ depend on the fluxes $f_A$ and $f_B$, as

$$S = s_A f_A = s_B f_B. \tag{3}$$

The dotted line in Fig. 5(c) shows the sticking coefficient of Zn, $s_{Zn}$, when we assume that all molecules of the minority species get incorporated ($s_{minority}=1$). This condition has been used in subsection B as a first order approximation of the growth rates.

In practice, the sticking probability of the minority species is smaller than unity. The data points in Fig. 5(c) represent the Zn sticking coefficient values (as a function of the atomic flux ratio) during ZnSe MBE at a substrate temperature of 300 °C.[14] The solid line corresponds to experimental data from Ref. 17, which we multiplied by a constant correction factor of 0.68 (=0.87/0.59). The reason for the introduction of this prefactor is to compensate for the overestimated values of Zn sticking coefficients in the latter (RHEED oscillation) study [$s_{Zn}=0.87$ at $p_{Se}:p_{Zn}=1.27$ (see Ref. 17). [The data of Ref. 14 are more reliable because the absolute value of the atomic flux was carefully determined from deposition rates at a low substrate temperature ($s_{Zn}=0.59$ at $p_{Se}:p_{Zn}=1.27$).[14]] With the correction factor incorporated, the solid line in Fig. 5(c) gives an excellent fit to the data points. We have used this curve to calculate the sticking coefficients of interacting Zn and Se species, in order to obtain the steady state flux distributions within the cavity of the mask.

For interacting molecules, the sticking coefficient $s(\mathbf{r},t)$ is a function of both time and position, because it depends on the distribution of the fluxes $f(\mathbf{r},t)$ of both components. Thus, Eqs. (1)–(3) describe a nonlinear problem, which can be solved taking into account this time-dependence. On applying Eq. (2) on Eq. (1), interchanging the summation with the integral, and applying Eq. (1) within the integral, leads us to the equation

$$f(\mathbf{r},t+\tau) = F_0(\mathbf{r}) + \int_{A_M} [1-s(\mathbf{r}',t)] f(\mathbf{r}',t) Z(\mathbf{r},\mathbf{r}') \times \frac{(\mathbf{n}_{r'r}\cdot\mathbf{n}')(\mathbf{n}_{rr'}\cdot\mathbf{n})}{(\mathbf{r}-\mathbf{r}')^2\pi} dA', \tag{4}$$

which describes the evolution of the total flux $f(\mathbf{r},t)$, in response of a change of the direct beam flux $F_0(\mathbf{r})$ (e.g., start of the mass-flow), as follows. The steady state flux distribution $f_\infty$ is obtained in the limit $t\to\infty$; i.e., by the iterative application of Eq. (3) and (4) on the time-dependent flux distribution $f(\mathbf{r},t)$. Without the time dependence, Eq. (4) becomes a continuity equation for the steady state. According to this continuity equation, the secondary flux $F_\infty=f_\infty-F_0$ is maintained in the steady state by the redistribution of the total flux $f_\infty$ (integral term).

### D. Surface diffusion and effective flux

In a previous study, Tomita *et al.* have observed that GaAs structures deposited through shadow masks form low-index facets at the edge.[9] Faceting of the edges (also known from SAE of III-V semiconductors on patterned substrates) can be understood as resulting from the surface diffusion of group-III adatoms. Surface migration results from gradients of the surface concentration $N_a$ of adatoms. The intrinsic dependence of $N_a$ and the diffusion coefficient $D$ on the surface orientation, thus causes *intersurface diffusion*, the prime factor leading to facet formation in III-V MBE.

From the diffusion model, it is known that the surface concentration $N_a=G\tau$ depends on the generation and the recombination of mobile adatoms, where the generation of surface atoms (with a rate $G$) corresponds to the impingement

of the group-III flux ($f_{III}$).[12,18] Recombination of surface adatoms means desorption of adatoms from the surface (lifetime $\tau_{des}$) as well as incorporation of adatoms into the solid phase (incorporation lifetime $\tau_{inc}$), hence the surface lifetime $\tau = (\tau_{des}^{-1} + \tau_{inc}^{-1})^{-1}$. However, in III-V MBE, desorption of adatoms is often negligible because of the low vapor pressure of group-III adatoms.

Hata *et al.*[12] have observed that the incorporation diffusion length $\lambda_{inc} = \sqrt{D\tau_{inc}}$ varies with the change of the arsenic flux $f_V$. When the group-V flux $f_V$ is high, the lifetime $\tau$ of group-III adatoms is reduced, because they react with the impinging group-V molecules. As a result, their surface concentration $N_a$ remains low. In the reverse case, $N_a$ becomes relatively high when the flux of group-V species is low. The surface diffusion of group-III adatoms within the cavity of a shadow mask is governed by the distribution of the group-V flux, according to the mass conservation equation

$$G - N_a/\tau - \nabla_S \cdot \boldsymbol{J}_S = 0, \tag{5}$$

wherein the first, second, and the third terms correspond to generation, recombination, and surface diffusion of the adatoms, respectively. $\nabla_S$ is the surface gradient operator and $\boldsymbol{J}_S = -D\nabla_S N_a$, the surface diffusion current of adatoms.

Equation (5) describes the planar redistribution of the surface atoms, which is governed by the flux distributions within the mask cavity [according to Eq. (4)]. Again, the flux distributions depend on the sticking coefficients, which in turn are modulated by the planar redistribution of the surface concentrations. In order to consider all these interactions, one has to find a solution to a system consisting of four redistribution processes. This becomes even more complex when two molecular species of one constituent element obey different surface kinetics, e.g., $As_2$ and $As_4$ molecules in III-V MBE.[19]

For the sake of simplicity, we restrict ourselves to the case in which the sticking coefficient of one (diffusing) species is about unity ($s_{III} \approx 1$), and the desorption lifetime of the other component is relatively short ($\tau_{des,V} \approx 0$), resulting, therefore, in a low surface diffusion of the latter. In addition, we assume that the group-V flux consists of a single molecular species (These are often good assumptions in III-V MBE at standard growth conditions.[19,21] In this case, we need to consider the redistribution of the flux of a single group-V species due to desorption [Eq. (4)], and the redistribution of group-III adatoms due to surface diffusion [Eq. (5)]. Analogously to Eq. (3), we equate the rates $S$ of group-III and group-V elements, as

$$S = s_V f_V = N_{a,III}/\tau_{inc,III}, \tag{6}$$

which gives us a system of equations [Eqs. (4)–(6)] with unique solution.

## IV. DISCUSSION

In this section, we discuss the implications of the interaction between the constituent species of compound materials, in the case of II-VI and III-V MBE through shadow masks. First, we discuss the effects of the surface reactions on the flux distribution (i.e., ZnSe MBE), and then we investigate how the flux ratio and the relative geometry of the fluxes and the mask affect the growth. Finally, we discuss the effects of interdependence of surface diffusion of one component and the flux distribution of the other, in the context of GaAs MBE. We also demonstrate the importance of such effects for SAE on patterned substrates.

For simplicity, we do not model the evolution of the growth interface, but restrict the discussion of MBE of compound materials to the initial growth geometry. Thus, we do not consider material deposits, which may affect the redistribution of secondary fluxes and diffusion currents in the mask cavity. Consequently, we also do not consider the evolution of the edges of the deposits, i.e., the self-formation of low-index facets, which is caused by the orientation dependence of surface kinetic processes.

### A. Interacting fluxes

Figure 5(d) shows a result of modeling the steady state flux distribution of Zn ($p_{Zn}$) and Se ($p_{Se} = 2 \times p_{Zn}$) fluxes in the same growth geometry as above [$(w,h,g,u) = (2,2,0,4)$; arbitrary units; $f_{Zn}$ and $f_{Se}$ are normalized to $p_{Zn}$]. The gray shaded curve shows the incorporation rate $S = sf$, its amplitude is proportional to the growth rate of ZnSe, as a function of the lateral position on the substrate.

The results for the total flux of interacting Zn and Se [see Fig. 5(d)] are similar to the dashed and solid lines in Fig. 5(b); i.e., noninteracting molecules with sticking coefficients of 0.5 and 0.1 for the minority and majority species, respectively. This "effective sticking coefficient" of the corresponding curves is a result of the interaction between the molecules: The majority species accumulates within the cavity of the mask. The increasing secondary flux of the majority species increases the sticking probability of the relative smaller number of minority molecules. This reduces the total flux of the minority species in the steady state, which in turn results in the sticking coefficient of the majority species being relatively low (as a result of the interaction).

Next, we consider a wide mask cavity ($u \gg h$). Mainly higher order fluxes $F_k$ with large ($k$) contribute to the total flux $f_\infty$ (secondary flux $F_\infty$) near the end walls of the mask cavity. Because of their relatively high sticking coefficient, the secondary flux of the minority species fades within a short distance from the aperture [as in Fig. 5(a)]. This in turn reduces the sticking coefficient of the majority species, which therefore becomes negligibly small ($s \approx 0$) at a large distance. Consequently, the secondary flux of the majority species in the steady state ($F_\infty$) is constant in this region. In contrast with the noninteracting case ($s = \text{const.} > 0$), it does not fade with the distance from the aperture.

### B. Change of the flux ratio

Next, we discuss the influence of a change of the growth conditions. By varying a single parameter in the standard growth conditions [$(w,h,g,u) = (2,2,0,4)$; $\varphi = \pm 14.0°$; $p_{Se}:p_{Zn} = 1.26 = 10^{+0.1}$], we predict growth rates in the Se domain ($R_{Se}$), the Zn domain ($R_{Zn}$), and beneath the Zn domain

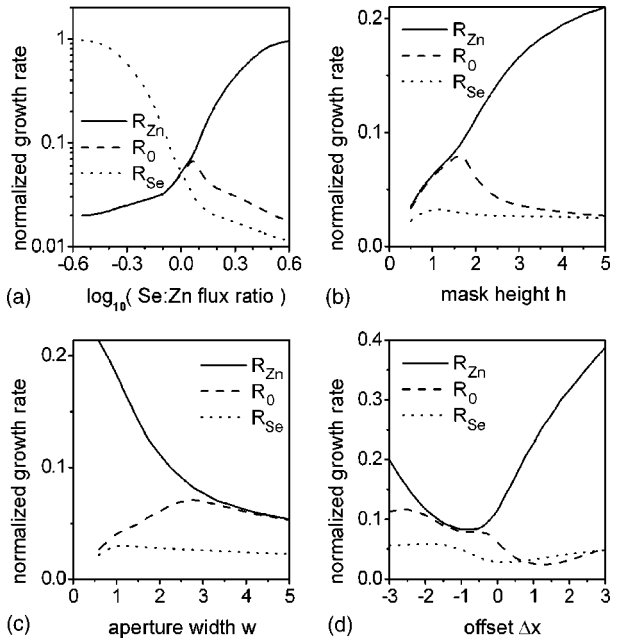


FIG. 6. Dependence of ZnSe growth rates in the Se domain ($R_{Se}$), the Zn domain ($R_{Zn}$), and without a direct beam ($R_0$) as a function of the growth conditions: (a) Change of the Se:Zn flux ratio. (b) Change of the mask height $h$. (c) Change of the aperture width $w$. (d) Change of the lateral position of the incidence regions of Zn and Se below the mask.

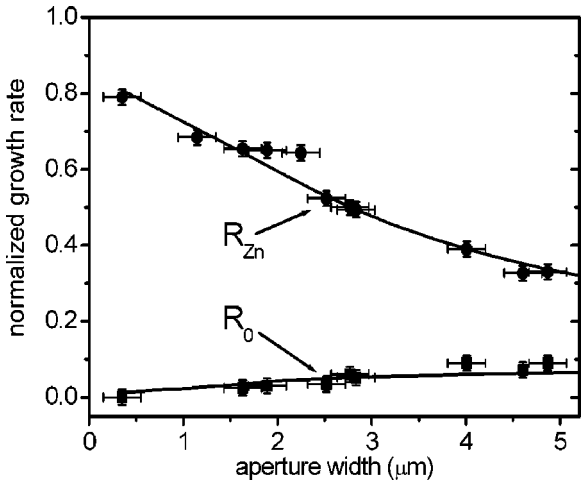


FIG. 7. Normalized ZnSe growth rates in the Zn domain ($R_{Zn}$) and outside of the Zn domain ($R_0$) dependent on the aperture width $w$. The solid lines show growth rates extracted from the model for an atomic flux ratio $\log_{10}(p_{Se}:p_{Zn})=+0.32$. The corresponding experimental data was obtained from sample #4.

($R_0$); i.e., without a direct beam [see Fig. 5(d)]. Figure 6 shows the calculated plots, normalized with respect to the growth rate without a shadow mask. The first plot in Fig. 6(a) shows the effect of a variation of the atomic flux ratio ($p_{Se}:p_{Zn}$), while the direct flux of the minority species maintained at $p_{minority}=1$ . The solid line shows that $R_{Zn}$ increases with increasing Se flux. Without sufficient Se overpressure [$\log(p_{Se}:p_{Zn})<+0.07$], the growth rates $R_{Zn}$ and $R_0$ are about equal (at the edge of the Zn domain) because on this side of the aperture of the mask ($x<0$) growth is limited by the secondary flux of Se. A Zn shoulder structure ($R_{Zn}>R_0$) is selectively formed when the secondary flux of Se exceeds that of Zn on both sides of the aperture of the mask [$\log(p_{Se}:p_{Zn})>+0.07$]. When the Se pressure is further increased ($p_{Se}:p_{Zn}\gg 1$), it finally exceeds the total Zn flux in the incidence region of Zn. ZnSe grows in the entire incidence region of Zn with a homogeneous growth rate, $R_{Zn}\approx 1$. While $R_{Zn}$ increases with the Se flux, the deposition rate $R_0$ (growth without a direct flux) decreases [see dashed line in Fig. 6(a)]. This is as a result of the interaction between Zn and Se; i.e., the suppression of Zn input (minority species) when excess Se (majority species) is accumulated within the cavity of the mask. The symmetric distribution of the curves $R_{Se}$ and $R_{Zn}$ in Fig. 6(a) with respect to an inversion of the flux ratio demonstrates that the interaction between the fluxes is important, rather than the individual material properties of Zn and Se.

The predictions of the model are in good agreement with the experiment as is demonstrated by samples #1, #2, #3, and #4 (see Fig. 1). Employing the dimensions of the shadow mask and the incidence angles of Zn and Se of each experiment in the model, we have determined the flux ratio at which $R_{Zn}$ matches the experimental growth rate of the shoulder structure. These determined logarithmic flux ratios, $\log(p_{Se}:p_{Zn})$, are +0.32, +0.05, −0.30, and −0.60, for samples #4, #1, #2, and #3, respectively, which is reasonable considering the change of the BEP ratio towards Zn-rich growth conditions.

Because of the coexistence of Zn and Se pressures within the cavity of the mask, ZnSe grows on the entire surface of the cavity. According to the model, the growth rate of ZnSe in the absence of a direct beam $R_0$ is in the range of 2%–4% of the growth rate in the overlap region. This again is in good agreement with the experiment (see Figs. 1 and 7).

In the case of sample #1, the growth rate within the overlap region is higher by a factor of 1.14 on the left hand side of the main structure [see Fig. 1(a)]. In contrast, a flat plateau is obtained in the overlap region of samples #2, #3, and #4 [see Figs. 1(b) and 1(c)]. The increase of the growth rate [sample #1], which is limited by the total Zn flux (minority species), can be attributed to the increase of secondary flux of Zn. In good agreement with the experiment, the model predicts an increase of the growth rate by a factor of 1.09 near the Zn domain, where Zn is still the majority species in the mask cavity. However, a substantial increase of the growth rate due to the increase of the secondary flux of the minority species is obtained only when the flux ratio is nearly stoichiometric. For higher flux ratios, the interaction between the fluxes suppresses the input of the minority species and a flat plateau is obtained [samples #2, #3, #4].

### C. Change of the growth geometry

In Figs. 6(b) and 6(c) we demonstrate the importance of the mask geometry. In these figures, one may observe that the accumulation of the majority species is strongly enhanced by an increase in the height $h$ of the shadow mask or a reduction of the aperture width $w$. Both these changes of

the mask geometry reduce the escape rate of molecules out of the cavity underneath the mask and thereby increase the interaction between the fluxes. In the extreme limits, $w \to 0$ and $h \to \infty$, the probability of the escape of molecules of the minority flux becomes negligibly small. Because of the pairwise extinction of molecules, the secondary flux of the majority species approaches $(p_{\text{majority}} - p_{\text{minority}})$ in the steady state.

A different way to modify the escape rate of molecules is by shifting the position of the incidence region on the substrate (changes in both the solid angle of the aperture and the effusion angle). Figure 6(d) shows the effect of a synchronic shift $\Delta x$ of the incidence regions of Zn $(\Delta x_{Zn} = -0.5 + \Delta x)$ and Se $(\Delta x_{Se} = +0.5 + \Delta x)$ relative to the aperture of the mask. For positive offsets $(\Delta x > 0)$, the escape of Se is reduced; i.e., its secondary flux of Se within the cavity is increased. On the other hand, shifts in the opposite direction $(\Delta x < 0)$ both reduce the escape of Zn and increase the escape of the majority species Se. This changes the ratio of the secondary flux within the cavity in such a way that at $\Delta x = -1$ no Zn shoulder is formed $(R_{Zn} \approx R_0)$ in spite of the Se-rich growth conditions [see Fig. 6(d)]. This demonstrates that the growth geometry is crucial for the growth regime below the mask. When the incidence regions are shifted deep underneath the mask $(\Delta x \to +\infty$ or $\Delta x \to -\infty)$, the escape of both species is minimized. Therefore, the problem is equivalent to $w \to 0$, $h \to \infty$, and the secondary flux of the majority species approaches a constant value $(p_{\text{majority}} - p_{\text{minority}})$ near the end walls of the mask cavity in the steady state.

Sample #4 was fabricated in order to validate the predictions of the model regarding a variation of the mask geometry: In a single growth experiment the aperture width $w$ was varied. Figure 7 shows the experimental data of the growth rates $R_{Zn}$ and $R_0$ (normalized to the growth rate without shadow mask) as a function of the aperture width $w$. The horizontal error bars are due to the closure of the aperture during overgrowth; i.e., a systematic error. We have extracted the theoretical values of $R_{Zn}$ and $R_0$ by modeling the growth regime based on the geometry of the experiment (incidence angles and mask dimensions). The only fitting parameter is the atomic flux ratio, which was set to $\log(p_{Se}:p_{Zn}) = +0.32$. As is shown by the solid lines in Fig. 7, the model gives an excellent fit of the experimental data for both the growth rate of the Zn shoulder structure $R_{Zn}$, and the growth rate without a direct flux $R_0$.

### D. Effects of surface diffusion

Here, we discuss the effects of interactions between the surface diffusion currents of group-III adatoms and the group-V fluxes in the mask cavity of the GaAs sample (see Fig. 3). An interesting observation is that the interface of the GaAs substrate is modulated without incidence of primary group-III species. According to Eq. (4), no surface diffusion should take place without a surface concentration $(N_a > 0)$ of group-III adatoms. Since $f_{III} \equiv 0$, a different generation process, which has not been considered in previous investigations of surface diffusion,[12,18,20] must cause the observed effects. We suggest that there exists a thermal generation process $g(T)$ that coincides with desorption of $As_2$ from the surface. In the case of the GaAs(001) surface, it was found that the outgoing $As_2$ flux exceeds the rate equivalent to 1 monolayer (ML)/s at temperatures above 600 °C.[21] This possibly generates weakly bonded Ga surface atoms at a rate $g$, which is of the same order. Thus, the total generation rate of adatoms is $G(\mathbf{r},T) = g(T) + f_{III}(\mathbf{r})$. Therefore, the thermal process results in an intrinsic contribution to the surface concentration of adatoms $N_i = g\tau$, which, however, does not increase the net growth rate. The net growth rate can then be calculated by $S = N_a/\tau_{inc} - g$.

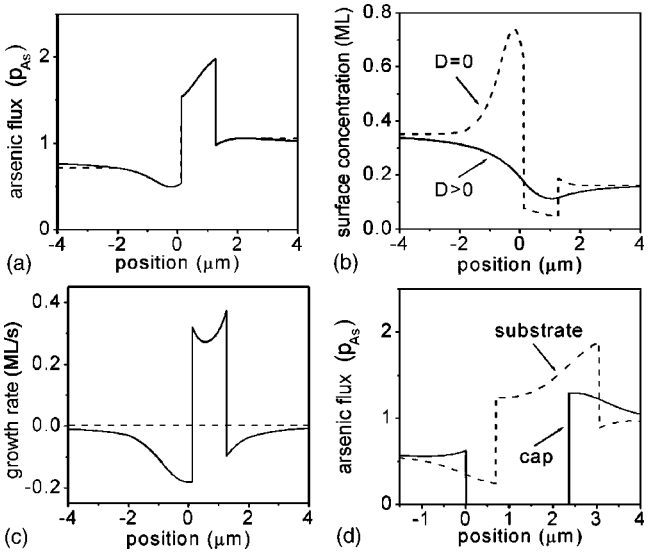


FIG. 8. Modeling of the surface diffusion of group-III adatoms dependent on the arsenic pressure. (a) Normalized arsenic flux in the case of the GaAs sample [see Fig. 3(a)]. (b) Intrinsic surface concentration of Ga adatoms with (solid curve) and without (dashed curve) surface diffusion. (c) Calculated growth rates caused by the surface diffusion, which is controlled by the arsenic flux. (d) Normalized arsenic flux on the substrate and on the underside of the mask in the case of the InAs sample (see Fig. 2).

During the thermal treatment of the GaAs sample, an As beam (mainly $As_4$ molecules) impinged through the mask aperture (see white lines in Fig. 3). Because no additional group-III flux was used in the experiment, we can assume that the effect of the group-III surface concentration on the redistribution of the group-V flux is limited. In particular, the sticking coefficient of group-V species is about zero in most areas of the cavity of the mask. Only in the incidence region of the direct beam a small fraction $(<10\%)$ of arsenic is incorporated in the structure, while areas with negative growth rate act as arsenic sources. Therefore, Eqs. (1) and (2) give a reasonable approximation of the distribution of arsenic fluxes when a constant sticking coefficient $s = 0$ of arsenic molecules is assumed. Figure 8(a) shows the arsenic flux distribution normalized with respect to the primary flux $p_{As} = 1.2 \times 10^{-5}$ Torr.

Nishinaga *et al.* has proposed that the incorporation lifetime of group-III adatoms, $\tau_{inc}$, varies as $f_V^{-\gamma}$, where $f_V$ is the arsenic pressure and $\gamma$ the reaction order of the incorporation process ($\gamma = 2$ in the case of III-V MBE with $As_4$ flux).[18] Figure 8(b) shows the surface concentration of group-III ada-

toms obtained by solving Eq. (5) for the flux distribution shown in Fig. 8(a). The solid line (dashed line) represents the surface concentration considering (neglecting) surface diffusion. For the calculation, the value of $g$, which does not affect the profile of the curves, has been assumed to be 0.25 ML/s, for reasons explained below. In the case of surface diffusion ($D>0$), $\lambda_{inc}$ is assumed to be 1.2 $\mu$m for $f_{As}=1.2\times10^{-5}$ Torr. This value is consistent with the results of microprobe RHEED experiments for a substrate temperature of 630 °C.[18] One may observe that the effect of the surface diffusion is pronounced in the regions where the concentration gradient $\nabla_S N_a$ is large, and the arsenic flux low; i.e., $\lambda_{inc}$ large.

The resulting growth rate curves $S=N_a/\tau_{inc}-g$ are presented in Fig. 8(c). The shape of the curve is in good agreement with the experimental surface profile [see Fig. 3(a)]. According to the model, and demonstrated by the experiment, positive growth rates are expected in the incidence region of the arsenic beam, while negative growth rates (etching rates), outside this region. However, both growth rate maxima are near the edges of the growth region.

This can be explained by the gradient of the group-V surface concentration, which results in a reverse gradient of the surface concentration of group-III adatoms, as shown in Fig. 8(b). Diffusion currents $\boldsymbol{J}_S$ from regions with low group-V secondary flux towards regions with high group-V pressure tend to reduce the gradient $\nabla_S N_a$. As a result of the planar redistribution, compound material grows only in the incidence region of arsenic on the substrate. The growth rate is negative in regions with low group-V pressure, which therefore act as a source of group-III atoms.

The gradient of the As flux also explains why deeper grooves are formed on the left-hand side of the structure shown in Fig. 3(a), while the maximum positive growth rate is observed at the right-hand side of the incidence region of arsenic. In the incidence region of arsenic, the total flux [see Fig. 8(a)] increases from left to right and hence causes a net diffusion current in the same direction. However, the diffusion currents at the edges of the incidence region are larger than that at the middle of the incidence region. Hence, there is a local maximum of the growth rate at the left limit, and an absolute maximum at the right limit of the incidence region.

According to Eq. (5), surface kinetics, such as the limited mobility of surface atoms ($D$) and their finite lifetime ($\tau$), limit the surface diffusion. Hence, diffusion currents decay exponentially with distance from the source, on a length scale equal to the incorporation diffusion length $\lambda_{inc}=\sqrt{D\tau_{inc}}$. This is analogous to intersurface diffusion during MBE on patterned substrates.

The surface concentration $N_a$ and, hence the growth rates $S$ in Fig. 8(c) scale with $g$. Therefore, $g$ can be determined by comparing the theoretically obtained growth rates with the experimental values. In our experiment the intrinsic generation rate is as high as $g\approx0.25$ ML/s. Hence, the thermal process generates surface adatoms with a rate that is comparable to typical impingement rates of group-III atoms in III-V MBE.

Unlike the GaAs sample, the intrinsic generation of Ga surface atoms is negligible in the case of InAs growth because of the relatively low substrate temperature. In this case, adatoms are generated by the beam of In atoms, which impinge on the GaAs mesa (between the black dashed arrows in Fig. 2). As can be seen in Fig. 2, the largest amount of InAs is deposited in the As-domain, where according to the model the arsenic flux is maximum. The corresponding flux distribution, as a function of the lateral position (on the substrate) is shown in Fig. 8(d) (dashed line). Obviously, the incorporated In adatoms migrate along the gradient of the arsenic flux from their area of incidence (between the black dashed arrows) to this region. In contrast, almost no InAs deposition takes place in the incidence region of the In flux. Only at the left limit of the incidence of arsenic, an InAs wire structure can be observed. This is caused by the diffusion current of In adatoms from the In domain. $\boldsymbol{J}_S$ is at maximum at the step edge of the arsenic flux where the gradient of the surface concentration of In surface atoms would be maximum without diffusion.

Based on the model, we can also understand the observations on the mask-cap (see Fig. 2). The solid curve in Fig. 8(d) shows the calculated flux distribution of arsenic on the lower surface (backside) of the mask's cap layer. Near the side walls of the mask cavity, the arsenic flux (solid line) approaches the same value as that of the flux on the substrate (dashed line). As a result of the non-normal incidence of the arsenic beam, the incidence region on the substrate is offset to the right (relative to the aperture). The secondary As flux on the backside of the cap, therefore, increases on the right wing. In particular, it is at maximum near the aperture and the calculated flux ($f_{As}>1.2p_{As}$) exceeds the primary flux ($p_{As}$) of the direct beam, which impinges on the top side of the cap. As a result of surface diffusion [Eq. (5)], In adatoms effectively diffuse from the top to the backside of the cap, which explains the observed InAs deposit on the undersurface of the right wing of the mask. In a $\sim3$ $\mu$m wide stripe on the mask, no InAs pyramids were formed, suggesting that the surface diffusion length of In adatoms exceeds this value in the experiment. In contrast, on the backside of the left wing of the mask, the secondary arsenic flux is slightly smaller ($f_{As}<0.8p_{As}$) than the direct beam flux. Because of this, there is no effective migration of In adatoms from the top side to the backside of the left wing.

## V. SUMMARY

In summary, we have studied growth features observed during molecular beam epitaxy of II-VI and III-V materials through epitaxial shadow masks. The investigation focused on the various shadow effects specific to the growth of compound materials. In order to explain the observations, we have developed a consistent model for the redistribution of the constituent species within the mask cavity, based on which we could predict the local growth rates. Under shadow masks, the species redistribute via (1) multiple desorption and (2) surface diffusion. The model relies upon specific properties of II-VI and III-V material systems, which describe the reactions at the growth interface. Based on these interactions between the constituent species, we could determine the distributions of the species within the mask cavity, at different growth conditions.

Due to the specific properties of II-VI materials, secondary fluxes of both group-II and group-VI species coexist in the mask cavity, and thus compound material deposits on the entire surface. Our model also predicts the formation of a shoulder structure in the domain of the minority-species flux, which was observed in experiments where ZnSe was grown through epitaxial shadow masks. We also investigated the effects of modulation of the flux ratio and manipulation of growth geometry, and found good agreements between experimental observations and calculated growth rates.

While the shapes of the II-VI deposits can be explained without considering surface diffusion, the profiles of the III-V deposits are governed by the redistribution of group-III adatoms via surface diffusion. However, the multiple desorption of group-V molecules, which causes secondary group-V flux in the mask cavity, also plays an important role and influences the group-III surface concentration. Based on these findings, we can understand shadow effects observed in the case of III-V materials.

## ACKNOWLEDGMENTS

The authors would like to acknowledge Suddhasatta Mahapatra, Professor Karl Brunner, and Professor Günther Bauer for their comments and suggestions, as well as the support by the Deutsche Forschungsgemeinschaft through SFB 410.

[1] W. T. Tsang and M. Ilegems, Appl. Phys. Lett. **31**, 301 (1977); W. T. Tsang, and A. Y. Cho, *ibid.* **30**, 293 (1977).

[2] H. Saito, I. Ogura, Y. Sugimoto, and K. Kasahara, Appl. Phys. Lett. **66**, 2466 (1995).

[3] G. M. Peake, L. Zhang, N. Y. Li, A. M. Sarangan, C. G. Willison, R. J. Shul, and S. D. Hersee, J. Vac. Sci. Technol. B **17**, 2070 (1999).

[4] Y. Luo, S. P. Guo, O. Maksimov, V. Asnin, F. H. Pollak, Y. C. Chen, and M. C. Tamargo, Appl. Phys. Lett. **77**, 4259 (2000).

[5] G. H. Döhler, G. Hasnain, and J. N. Miller, Appl. Phys. Lett. **49**, 704 (1986).

[6] A. Lorke, J. H. English, A. C. Gossard, and P. M. Petroff, J. Appl. Phys. **77**, 3578 (1995).

[7] T. Schallenberg *et al.*, Appl. Phys. Lett. **82**, 4349 (2003); T. Schallenberg *et al., ibid.* **83**, 446 (2003); T. Schallenberg, C. Schumacher, K. Brunner, and L. W. Molenkamp, Phys. Status Solidi B **241**, 564 (2004); T. Schallenberg, T. Borzenko, G. Schmidt, L. W. Molenkamp, S. Rodt, R. Heitz, D. Bimberg, G. Karczewski, J. Appl. Phys. **95**, 311 (2004); T. Schallenberg, L. W. Molenkamp, S. Rodt, R. Seguin, D. Bimberg, and G. Karczewski, Appl. Phys. Lett. **84**, 963 (2004).

[8] T. Schallenberg, C. Schumacher, and L. W. Molenkamp, Phys. Status Solidi A **195**, 232 (2003).

[9] N. Tomita, N. Yoshida, S. Shimomura, K. Murase, A. Adachi, and S. Hiyamizu, J. Cryst. Growth **150**, 377 (1995).

[10] T. Nishikawa, M. Kubo, and Y. Sasai, Appl. Phys. Lett. **68**, 3428 (1996).

[11] C. Schumacher and W. Faschinger, J. Cryst. Growth **214/215**, 732 (2000).

[12] M. Hata, A. Watanabe, and T. Isu, J. Cryst. Growth **111**, 83 (1991).

[13] T. Schallenberg, C. Schumacher, and W. Faschinger, Physica E (Amsterdam) **13**, 1212 (2002).

[14] J. Riley, D. Wolfframm, D. Westwood, and A. Evans, J. Cryst. Growth **160**, 193 (1996).

[15] Equations (1) and (2) can also be found in a similar form in Ref. 22. Drotar *et al.* have modeled roughening of the growth interface, which takes place during the sputtering deposition and etching processes as a result of shadowing and desorption of molecules. In this case, the surface was almost planar and consequently only $F_k(k<2)$ had to be considered. In contrast, for the shadow effects discussed here, higher order fluxes $F_k$ up to orders $k>100$ may contribute significantly to the total flux in the mask cavity and can therefore not be omitted.

[16] D. Wolfframm, D. A. Evans, D. I. Westwood, and J. Riley, J. Cryst. Growth **216**, 119 (2000).

[17] P. Ruppert, D. Hommel, T. Behr, H. Heinke, A. Waag, and G. Landwehr, J. Cryst. Growth **138**, 48 (1994).

[18] T. Nishinaga, X. Q. Shen, and D. Kishimoto, J. Cryst. Growth **163**, 60 (1996); M. Hata, T. Isu, A. Watanabe, and Y. Katayama, J. Vac. Sci. Technol. B **8**, 692 (1990).

[19] C. T. Foxon and B. A. Joyce, Surf. Sci. **50**, 434 (1975); C. T. Foxon and B. A. Joyce, *ibid.* **64**, 293 (1977).

[20] D. Kishimoto, T. Nishinaga, S. Naritsuka, and H. Sakaki, J. Cryst. Growth **240**, 52 (2002).

[21] S. Yu. Karpov and M. A. Maiorov, Surf. Sci. **344**, 11 (1995).

[22] J. T. Drotar, Y.-P. Zhao, T.-M. Lu, and G.-C. Wang, Phys. Rev. B **61**, 3012 (2000); **62**, 2118 (2000).